Imaging Human Body Down to Molecular Level

Hans Deyhle, Georg Schulz and Bert Müller
Biomaterials Science Center (BMC), University of
Basel, Basel, Switzerland

Synonyms

Three-dimensional imaging of human tissues

Definition

The human body consists of nanometer-sized units, including proteins, apatite crystallites, collagen, and myelin fibers. Imaging, here, means the identification, localization, and quantification of these units within the human body.

Overview

The human body consists of about 10^{27} molecules. This number is so huge that it is impossible to determine their location or even only to store this amount of data. Using a logarithmic scale (see Fig. 1), one realizes that a biological cell with an extension of about 10 μm includes as many molecules like the human body biological cells. Even the number of cells within the human body is huge and beyond our imagination. The number of stars in the Milky Way, for example, is thousand times smaller than this number. Therefore, for imaging the human body on the nanometer scale, one has to restrict to predefined parts of the body or to take advantage of symmetries or periodicities as known from the atomic view of single crystals in solid state physics.

Three-dimensional (3D) imaging in daily clinical practice of well-equipped hospitals reaches a spatial resolution of a fraction of a millimeter, as indicated by the magnetic resonance imaging (MRI) in Fig. 1. Hence, the spatial resolution of medical imaging facilities is far from that of molecular scale. In engineering and research, however, methods are known that allow imaging structures down to the world of atoms. As shown in the overview of Fig. 1 micro computed tomography (μCT) well established in materials science yields a spatial resolution as low as a fraction of a micrometer in real space. The necessary dose for the subcellular level, however, is so high that only *post-mortem* studies are permitted. Although the spatial resolution is high enough to visualize individual biological cells, the contrast is, contrary to hard tissues, too low. Monochromatic X-ray beams, as applied in synchrotron radiation-based μCT (SRμCT), provide much better contrast. Therefore, SRμCT has recently allowed visualizing individual cells in human tissue after appropriate staining [1]. Very recently, grating-based phase-contrast SRμCT has been introduced, which gives rise to even orders of magnitude better contrast for human soft tissues [2]. Here, non-stained, individual Purkinje cells located in brain come to light (see Fig. 1). In order to make visible nanostructures between 1 and 100 nm in real space, however, X-ray optics has to be integrated into the setup, and the accessible volumes become as small as for electron-based techniques.

Imaging Human Body Down to Molecular Level, Fig. 1 The selected imaging techniques (MRI, SRμCT, SAXS/WAXS) cover different length scales down to the molecular level
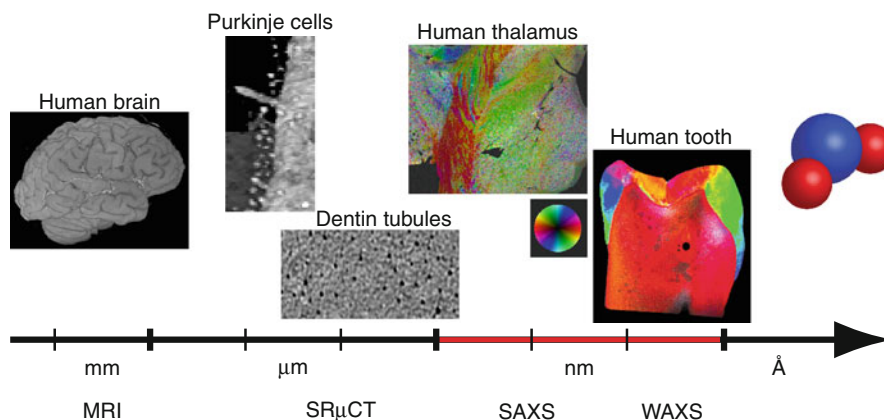
Diffraction and scattering methods are established techniques to quantitatively characterize the arrangements of atoms or molecules in reciprocal space [3]. Therefore, they give rise to average values within the illuminated volume. The combination of small probing beams and scanning provides spatially resolved data for the nanometer range and below. X-ray based methods are especially suitable for human tissues. They are termed scanning small-angle X-ray scattering (scanning SAXS) and scanning wide-angle X-ray scattering (scanning WAXS). While SAXS covers the entire nanometer range, WAXS depicts the interatomic distances on the sub-nanometer scale (see Fig. 1).

Basics

X-ray computed tomography (CT) is a widespread imaging technique in the radiology. Multi-slice CT (MSCT), for example, is used to identify tumors and to plan radiation therapy treatments. In dental medicine, cone-beam computed tomography (CBCT) is a standard imaging technique. The 3D images are used, for instance, to decide if enough bone is present for implant placements. Figure 2 shows, as an example, the 3D rendering of a part of a human skull acquired with the Accuitomo 80 CBCT system (Morita, Kyoto, Japan) recorded with an acceleration voltage of 70 kV and a beam current of 4 mA. Five hundred and twelve radiographs were acquired over $360°$. The voxel size of the tomography data was $0.25 \times 0.25 \times 0.16$ mm^3.

To improve the spatial and density resolution of the X ray–based imaging techniques, dangerous doses are


Imaging Human Body Down to Molecular Level, Fig. 2 The 3D rendering of a human skull generated from CBCT data impressively shows the different hard tissues of teeth and bone

required and in vivo measurements impossible. Hence, methods such as μCT are rather found in the field of materials science than medicine. Nevertheless, *postmortem* studies are common in many research laboratories and provide exhaustive morphological information on the micrometer scale. Several μCT-systems are built at synchrotron radiation facilities,

Imaging Human Body Down to Molecular Level, Fig. 3 Layout of a synchrotron radiation facility consisting of a storage ring, an insertion device, and the end-station for tomographic imaging
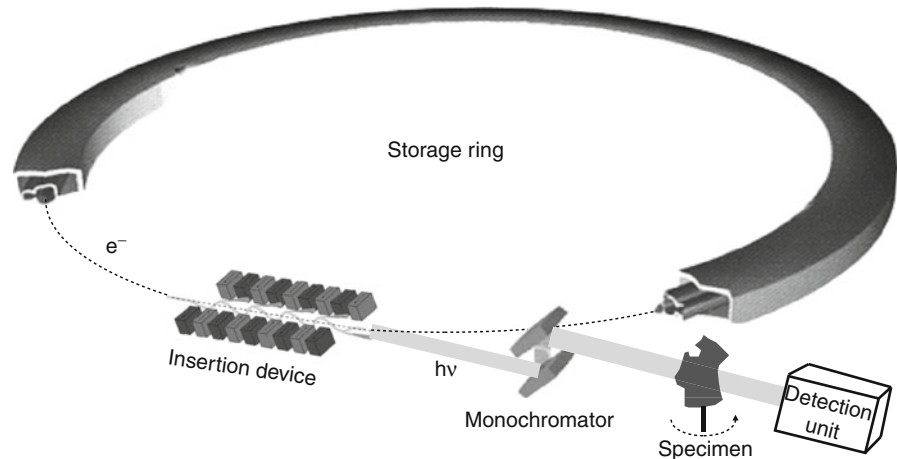
which provide highly brilliant X-rays for different kinds of imaging purposes. The main components of such a facility are schematically represented in Fig. 3. The highly energetic electrons or positrons circulate in the storage ring and through insertion devices, where the intense X-ray beams are generated. The insertion devices are classified as bending magnet (first generation), wiggler (second generation), undulator (third generation), and free-electron laser (fourth generation). The difference of the insertion devices is – besides the increasing intensity – inter alia, the incoherent (first and second generation) and coherent (third and fourth generation) interference of the produced X-rays. The high intensity of synchrotron light allows realizing a tunable X-ray source. For that, a monochromator selects the predefined photon energy. The μCT end-station contains the sample manipulator and the detector.

The high X-ray intensity allows pushing the resolution of tomography at synchrotron radiation sources toward the sub-micrometer range, at cost, however, of a reduced field of view. Figure 4 illustrates the SRμCT imaging capabilities for a polymer cast of the vascular system from a human C51 tumor, acquired at the TOMCAT beamline (Swiss Light Source, Paul Scherrer Intstitut, Switzerland) at a photon energy of 15 keV. In the top image, the isotropic voxel length corresponds to 5.9 μm. With these settings, the whole tumor became visible. Capillaries with a diameter smaller than 10 μm, however, are not identified. Therefore, local tomography is often performed as demonstrated on the image of the same tumor below. Here, only a part of the specimen is scanned. The voxel

length corresponded to 0.74 μm, and even the smallest capillaries having a diameter below 4 μm can be recognized.

Absorption tomography, as described above, is particularly suited for hard tissues like bone or teeth as these provide enough contrast in the X-ray images. For soft tissues, e.g., human brain, absorption-contrast SRμCT has a limited success because the different soft tissues generally present very similar X-ray absorption properties. For this kind of tissue, phase-contrast SRμCT promises excellent results where, contrary to the absorption contrast, the real part of the refractive index often expressed in terms of its decrement from unity, $\delta(x,y,z)$, is measured. For X-ray energies far away from the absorption edges, it relates to the electron density distribution $\rho_e(x,y,z)$:

$$\delta(x,y,z) = \frac{r_e \lambda^2}{2\pi} \rho_e(x,y,z) \qquad (1)$$

with r_e denotes the classical electron radius and λ the X-ray wavelength [4]. In particular, a very high sensitivity can be reached by the recently developed grating-based phase-contrast SRμCT [4]. A schematic view of the setup is given in Fig. 5. The grating interferometer is composed of a beam-splitter grating g_1, consisting of silicon stripes with periodicity p_1, and an analyzer grating g_2, consisting of strongly X-ray absorbing stripes, often gold, with periodicity p_2. The periodicity of the grating g_2 has the half value of p_1. The grating g_1 induces a periodic fringe pattern in the X-ray wave-front intensity distribution with extreme values of the contrast at so-called Talbot distances
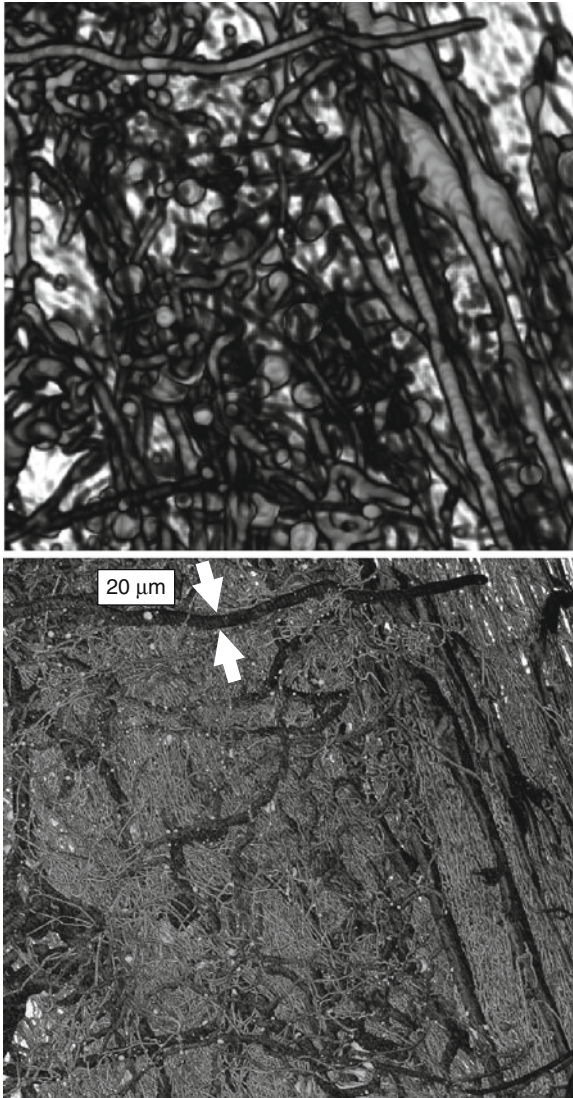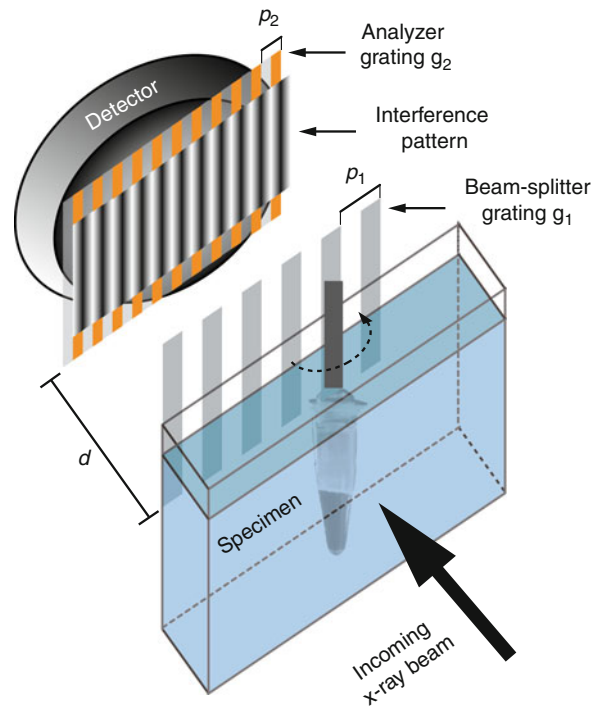
Imaging Human Body Down to Molecular Level, Fig. 4 Cast of the vascular network of a C51 tumor visualized by SRµCT – top global tomography; bottom local tomography

Imaging Human Body Down to Molecular Level, Fig. 5 Scheme of a grating-based interferometer for X-ray imaging at a third-generation synchrotron radiation source

from the beam-splitter grating. The Talbot distances are found at

$$d_n = \frac{n p_1^2}{8\lambda}, \quad (2)$$

where n is a positive integer. The intensity difference between fringe maxima and minima is largest at odd Talbot orders, while it is vanishing at even values of n [5]. When performing a phase-contrast µCT experiment, the distance between g_1 and g_2 is adjusted to

a Talbot distance with odd Talbot order. A specimen in the beam slightly deflects the incoming X-rays according to its refractive index distribution and leads to a disturbed fringe pattern. The analyzer grating permits detecting these changes using the phase-stepping method, where several images at different grating g_2 positions are recorded [4]. The quantitative relation between the local beam propagation $\alpha(y,z)$, the wave phase shift $\Phi(y,z)$, and the decrement of X-ray refractive index $\delta(x,y,z)$ can be obtained by equation

$$\alpha(y,z) = \frac{\lambda}{2\pi} \frac{\partial \Phi(y,z)}{\partial y} = \int_{-\infty}^{\infty} \frac{\partial \delta(x,y,z)}{\partial y} dx. \quad (3)$$

The investigation of human tissue in the nanometer range by means of X-rays is available through scattering experiments, which belong to the reciprocal imaging techniques (see also Study Nanomaterials/Nanostructures Using Small Angle Scattering, 00118). In SAXS experiments, a focused X-ray beam is scattered to small angles between approximately 0.2 and 20 mrad. In order to record these angles with

Imaging Human Body Down to Molecular Level, Fig. 6 Schematic representation of the information obtained from small-angle X-ray scattering measurements
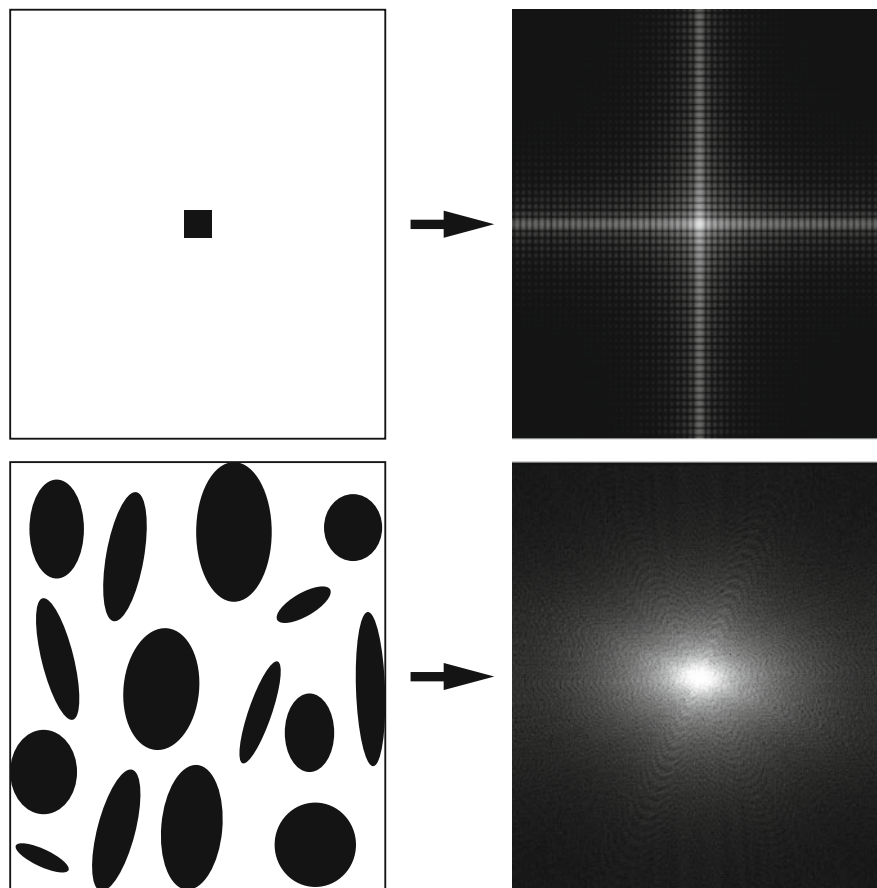
enough precision, the distance between specimen and detector amounts to several meters. The scattering signal is closely related to the Fourier transform of the electron density distribution of the specimens [3]. Figure 6 shows a schematic representation of the relationship between specimens (on the left) and scattering signal (on the right). In the first example of Fig. 6, the particle that causes the scattering signal cannot easily be recognized from the scattering pattern. The information concerning particle shape, size, and orientation, however, can be extracted. When different particles scatter simultaneously, the generated signal contains contributions from all of them, yielding a mean value from the illuminated volume.

The recent development of sophisticated detectors [6] enables the acquisition of several tens scattering patterns per second, allowing collecting scattering data over macroscopic areas in short time with a scanning approach [7]. Figure 7 elucidates the principle of scanning SAXS. A micro-focus X-ray beam is raster-scanned along *x*- and *y*-directions, while the scattering signal is recorded. Scanning with steps of several 10 μm, the nanostructure of the specimen in reciprocal space is revealed with micrometer resolution in real space.

Key Research Findings

Grating-based phase-contrast SRμCT provides excellent measurement sensitivity for soft tissues. Figure 8 shows three virtual cuts of a human cerebellum acquired at the beamline ID19 (European Synchrotron Radiation Facility, France) [8] in phase-contrast mode with a photon energy of 23 keV. For the experiment, the specimen was fixated in 4% formalin solution. The period of the beam-splitter grating was $p_1 = 4.785 \, \mu m$ and of the analyzer grating $p_2 = 2.400 \, \mu m$. The experiment was carried out at the ninth Talbot distance, thus a distance of $d = 479.4$ mm between the two gratings
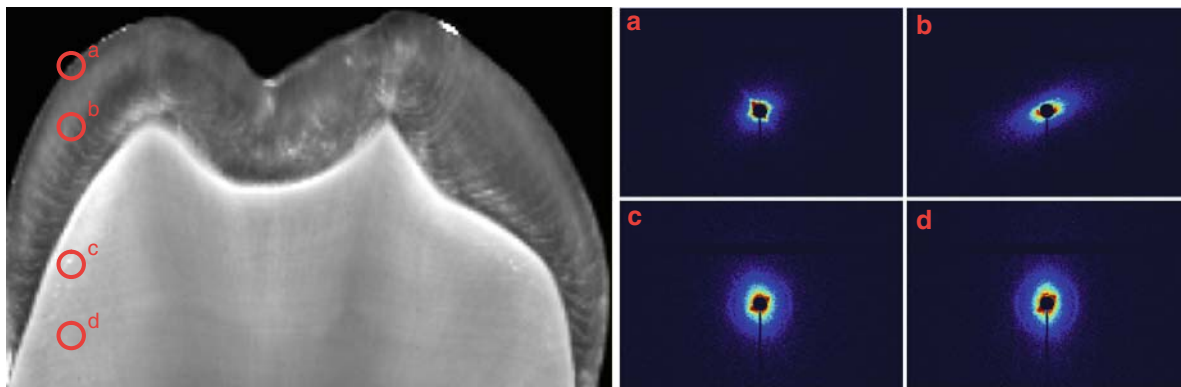
Imaging Human Body Down to Molecular Level, Fig. 7 Principle of scanning SAXS, elucidated on a tooth slice. The specimen is raster-scanned through the beam and at each raster point a SAXS pattern is recorded. On the right, the scattering patterns corresponding to points a through d are shown
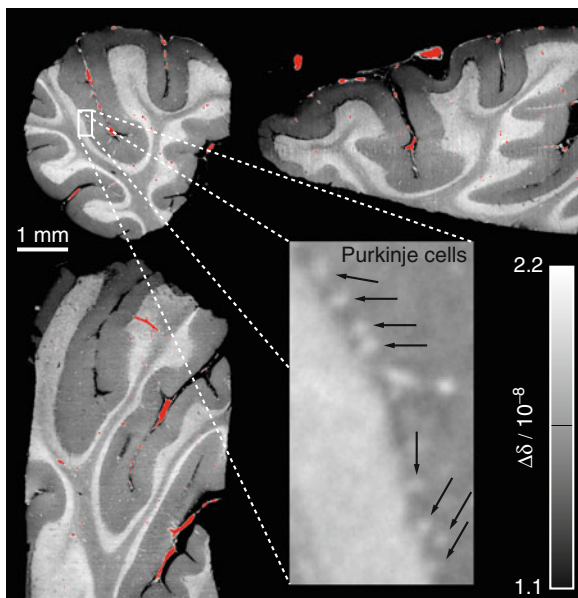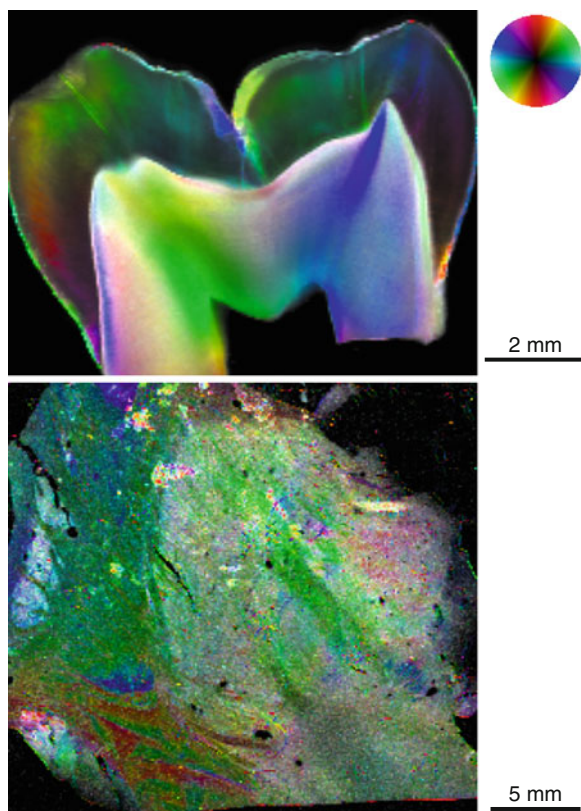

Imaging Human Body Down to Molecular Level, Fig. 8 Three orthogonal virtual cuts of a human cerebellum acquired at the beamline ID19 (European Synchrotron Radiation Facility, France) using grating-based phase-contrast SRμCT. The red-colored structures correspond to blood vessels. The inset illustrates the visualization of individual, non-stained Purkinje cells having diameters of around 50 μm

was adjusted. The Eppendorf container with the cerebellum in formalin solution was fixed on the high-precision rotation stage and immersed in a water bath (see Fig. 5) in order to minimize artifacts owing to X-ray phase curvature induced by the container surface. For the detection, a lens-coupled scintillator and

charge-coupled device (CCD) system using a FReLoN 2 K (Fast-Readout, Low-Noise, ESRF Grenoble, France) CCD with $2,048 \times 2,048$ pixels with the effective pixel size of 5.1 μm was used. Four phase-stepping images were taken over one period of the interferometer fringe pattern at each projection angle. With an exposure time of 1 s per image, 1,501 radiographs were recorded over a range of $360°$. The spatial resolution of the experimental data was estimated by means of Fourier analysis. The calculation resulted in (16.5 ± 0.5) μm for the processed projections and (20 ± 1) μm for the reconstructed tomogram. Figure 8 demonstrates that the phase contrast results allow for a clear differentiation between white (inner gray colored layer) and gray matter, and even a distinction within the gray matter, namely the stratum moleculare (dark region of the gray matter) and the stratum granulosum (bright region of the gray matter). The red-colored regions correspond to blood vessels. The inset in Fig. 8 illustrates the visualization of individual Purkinje cells, which underlines the performance of the technique in *post-mortem* brain imaging. The detection of individual Purkinje cells with spherical diameters of 40–70 μm in the surrounding soft tissues without the application of any stain or contrast agent is a novelty in CT imaging [2].

Human tissues often exhibit strong structural anisotropies of their nanometer-sized components, which are usually related to their function. SAXS allows inspecting hard and soft tissues [9], as illustrated in Fig. 9, where processed data from a slices of a human molar (top image, scattering from 162 to

Imaging Human Body Down to Molecular Level, Fig. 9 Processed SAXS data of slices of a human molar in the range corresponding to 162–183 nm and of a human thalamus in the range between 98 and 110 nm

183 nm features) and of a human thalamus (bottom image, scattering from 98 to 110 nm features) are shown. The mean orientation of the scatterers is according to the color wheel. The brightness relates to the abundance of nanostructures in the corresponding ranges, while color saturation codes the nanostructures anisotropy (cp. Chapter "Nanodentistry"). The tooth was scanned at a photon energy of 18.6 keV with 50 μm raster scan steps in both x- and y-directions, while the thalamus data were acquired at 11.2 keV with a step width of 75 μm. For both experiments, the distance between specimen and detector was set to 7.1 m. The scanning SAXS measurements reveal a high degree of anisotropy on the nanometer level in the tooth hard tissues. The orientation of the calcium phosphate crystallites in the enamel is found to be mainly perpendicular to the tooth surface, thus pointing in the direction of maximal

mechanical load. The crystallites in dentin are, however, mainly oriented parallel to the tooth surface. It is assumed that this organization is responsible for the extraordinary mechanical performance and lifetime of human teeth. The bright region on the right-hand side of the brain slice of Fig. 9 is the thalamus, which consists mainly of gray matter, and the so-called nuclei, which belong to the central nervous system. Within the thalamus, only a few small regions containing highly oriented nanostructures can be found. In contrast to gray matter, white matter consists of long myelinated nerve cells (axons), which transfer the nerve impulses between the nuclei. This tissue can be seen on the left-hand side of the brain slice, where the colors are saturated.

Future Research Directions

The human body is fascinating because of its huge complexity. Clinical CT-facilities reach a fraction of a millimeter. This limit will not be much shifted toward true micrometer scale, as (1) the amount of data has to be (semi-)automatically analyzed and (2) the dose becomes dangerous for the patient. Dose reduction has been one of the major research topics in clinical CT. For *post-mortem* visualization, μCT in absorption-contrast mode has been developed to a standard technique. The contrast for soft tissues is so weak that phase-contrast methods are required. Fine-tuning of the most advanced systems is a prerequisite to reveal cellular structures within the different organs of the human body. For the visualization of the nanostructures, however, scattering methods seem to be much better suited. Here, not just 2D-projection data, but also tomography data with reasonable real-space spatial resolution have to be acquired. Again, powerful software tools have to be realized for the treatment of the huge amount of data and to extract the nanometer-sized features of interest.

The structural information of the human body down to the nanometer level will provide a sound basis for developing nature-analogue biomaterials and biomimetic implants [10] to be launched for the benefit of patients. These biomimetic products will exhibit micro- and nanostructures, including their preferential orientation (anisotropy) as found in nature and revealed by highly advanced imaging techniques applying sophisticated software tools for data

I

treatment and medical image analysis. Learning from nature will lead to solutions of health problems in our aging society.

Cross-References

▶ AFM in Liquids
▶ Angiogenesis
▶ Atomic Force Microscopy
▶ Bioinspired Synthesis of Nanomaterials
▶ Biomimetics
▶ Electron Microscopy of Interactions Between Engineered Nanomaterials and Cells
▶ Microfabricated Probe Technology
▶ Models for Tumor Growth
▶ Nanodentistry
▶ Nanomechanical Properties of Nanostructures
▶ Nanomedicine
▶ Nanostructured Functionalized Surfaces
▶ Nanotechnology in Cardiovascular Diseases
▶ Scanning Electron Microscopy
▶ Selected Synchrotron Radiation Techniques
▶ Self-repairing Materials

References

1. Lareida, A., Beckmann, F., Schrott-Fischer, A., Glueckert, R., Freysinger, W., Müller, B.: High-resolution X-ray tomography of the human inner ear: synchrotron radiation-based study of nerve fiber bundles, membranes, and ganglion cells. J. Microsc. **234**(1), 95–102 (2009)
2. Schulz, G., Weitkamp, T., Zanette, I., Pfeiffer, F., Beckmann, F., David, C., Rutishauser, S., Reznikova, E., Müller, B.: High-resolution tomographic imaging of a human cerebellum: Comparison of absorption and grating based phase contrast. J. R. Soc. Interface **7**(53), 1665–1676 (2010)
3. Guinier, A., Fournet, G.: Small Angle Scattering of X-rays. Wiley, New York (1955)
4. Weitkamp, T., Diaz, A., David, C., Pfeiffer, F., Stampanoni, M., Cloetens, P., Ziegler, E.: X-ray phase imaging with a grating interferometer. Opt. Express **13**(16), 6296–6304 (2005)
5. Weitkamp, T., David, C., Kottler, C., Bunk, O., Pfeiffer, F.: Tomography with grating interferometers at low-brilliance sources. Proc. SPIE **6318**, 63180S (2006)
6. Heinrich, B., Bergamaschi, A., Brönnimann, C., Dinapoli, R., Eikenberry, E.F., Jhonson, I., Kobas, M., Kraft, P., Mozzanica, A.: PILATUS: A single photon counting pixel detector for X-ray applications. Nucl. Instrum. Meth. Phys. Res. A **607**, 247–249 (2009)
7. Bunk, O., Bech, M., Jensen, T.H., Feidenhans'l, R., Binderup, T., Menzel, A., Pfeiffer, F.: Multimodal x-ray scatter imaging. New J. Phys. **11**, 123016 (2009)
8. Weitkamp, T., Tafforeau, P., Boller, E., Cloetens, P., Valade, J.-P., Bernard, P., Peyrin, F., Ludwig, W., Helfen, L., Baruchel, J.: Status and evolution of the ESRF beamline ID19. AIP Conf. Proc. **1221**, 33–38 (2010)
9. Müller, B., Deyhle, H., Bradley, D., Farquharson, M., Schulz, G., Müller-Gerbl, M., Bunk, O.: Scanning x-ray scattering: Evaluating the nanostructure of human tissues. Eur. J. Nanomed. **3**, 30–33 (2010)
10. Müller, B.: Biomimetics and medical implementations. In: Bar-Cohen, Y. (ed.) Biomimetics: Nature-Based Innovation. CRC Press/Taylor & Francis Group (2011)

Immersion Lithography

Roger H. French
Department of Materials Science and Engineering,
Case Western Reserve University, Cleveland,
OH, USA

Synonyms

High index fluid immersion; Liquid Immersion lithography; Optical lithography by liquid immersion

Definition

Immersion lithography utilizes liquids with refractive indices >1 (the index of air) to enable sub-45-nm feature size (or half-pitch) patterning for semiconductor integrated circuits. An alternative to conventional "dry" optical lithography offering finer features, this method employs innovative materials at both the photomask and imaging stack levels.

Overview

In addition to the entries on Lithography and Immersion Lithography Materials, herein, the reader is directed to two recent review papers which surveyed the state of the art in immersion lithography, including photomasks and wafer level materials [1] and immersion lithography tools [2].